Sensors and Materials, Vol. 35, No. 9 (2023) 3151–3160
MYU Tokyo

S & M 3381

Low Retention Force of Water Droplet on Silicone Surface with Uniaxial Microgroove Structure Utilizing Molding Process

Kenji Yanagisawa[1*] and Chinatsu Saito[2]

[1]Department of Engineering, National Institute of Technology, Nagano College,
716, Tokuma, Nagano-shi, Nagano 381-8550, Japan
[2]Department of Engineering, Tottori University,
4-101, Minami Koyama, Tottori-shi, Tottori 680-8550, Japan

(Received April 25, 2023; accepted July 3, 2023)

Keywords: retention force, water droplet, sliding behavior, silicone, groove structure

Inspired by the water-repellent and self-cleaning properties of the lotus leaf in the natural world, artificial superhydrophobic surfaces have attracted extensive interest in academia and industry. Static and dynamic hydrophobicities are very important phenomena in our daily life as well as in many industrial processes. However, the difference between these two phenomena has not been well understood. The objective of this study was to investigate and predict the sliding behavior of water droplets on silicone sheet surfaces with uniaxial groove structures. The groove structures were fabricated on silicone sheet surfaces by a molding process using three different molds with different groove widths. Increasing the groove width decreased the sliding angle. The sliding angle could be reduced to a greater extent than that of previously reported fluorinated hydrophobic surfaces, which exhibited sliding angles of less than 2°. The retention force between the water droplet and the silicone sheet surface was proportional to the contact ratio. It was found that the retention force was proportional to the shape of the water droplet on the surface at the sliding angle, especially the product of the contact angle hysteresis and the width of the contact line.

1. Introduction

The importance of dynamic hydrophobicity is increasing across various industrial sectors, including vehicle development and semiconductor processes.(1) Dynamic hydrophobicity is associated with the removal performance of liquid droplets on solid surfaces. The sliding angle α, a traditional wetting parameter representing the dynamic hydrophobicity of a surface, is defined as the minimum inclination angle at which a droplet starts to move on the surface. When the surface is inclined at the sliding angle α, the droplet experiences deformation and tilts in the direction of the unbalanced gravitational force [Fig. 1(a)]. In particular, the front and rear ends of the droplet correspond to the contour of the interface in the direction of the unbalanced gravitational force, as illustrated in Fig. 1(b). The equilibrium behavior in this critical state is

*Corresponding author: e-mail: k_yanagisawa@nagano-nct.ac.jp
https://doi.org/10.18494/SAM4466

ISSN 0914-4935

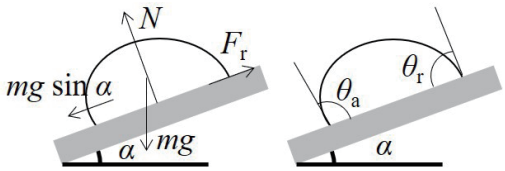

(a) (b)

Fig. 1. (a) Schematic illustration of the forces acting on a droplet and (b) the contour of the drop on the sliding angle α.

determined by the interaction between two forces: (i) gravity, which aims to deform and displace the droplet, and (ii) the force arising from the substrate due to contact angle hysteresis, which opposes the droplet's movement. These two forces are referred to as the critical force (F_c) and the retention force (F_r), respectively.[2]

Bikerman demonstrated a correlation between the width of the contact line of solid surfaces and water droplets (hereafter referred to as the contact-line width) and the sliding angle.[3] Subsequently, Furmidge showed that the difference in the cosines of the front and rear contact angles correlates with the sliding angle.[4] Consequently, from several subsequent studies, the sliding angle α is often expressed as Eq. (1).[5–9]

$$mg \sin \alpha = 2r\kappa\gamma \left(\cos \theta_r - \cos \theta_a \right) \tag{1}$$

Here, $2r$ is the contact-line width, k is a value dependent on the surface material between the solid surface and the water droplet, γ represents the surface tension of water, m is the mass of the water droplet, and g is the gravitational acceleration. θ_a and θ_r are referred to as the advancing and receding contact angles, respectively, and the difference in the cosines of the advancing and receding contact angles is called contact angle hysteresis (CAH).[2] Elsherbini and Jacobi[8] stated that k can be represented as $24/\pi^3$ from experiments and calculations, which is supported by the findings of Extrand.[9]

Several methods for controlling the value of k in Eq. (1) have been proposed in the literature. David and Neumann demonstrated through simulations that when a hydrophilic coating is applied in a line pattern, water droplets on the coated surface elongate along the direction of the lines.[10] Song *et al.* showed that when two types of fluorine coating are applied in alternating line patterns, the contact angle measured parallel to the lines is greater than that measured orthogonal to the lines.[11] Yoshimitsu *et al.*'s surface with fluorine-coated lines and grooves demonstrated that the contact angle measured parallel to the lines is larger than that measured orthogonal to the lines.[12] These findings suggest that it is possible to reduce the value of k by introducing line patterns on solid surfaces. However, no studies have evaluated the dynamic hydrophobicity of surfaces with line-patterned structures on silicone-based materials.

Lotus leaves exhibit superhydrophobic surfaces, which is why their surfaces are always clean.[13] The surface of rose petals has a strong adhesion to water droplets, so the droplets are not removed even when the petals are turned upside down.[14,15] Wang and Bhushan investigated

the water droplet removal properties of several superhydrophobic surfaces with contact angles exceeding 150°.[16] The CAH of these superhydrophobic surfaces varied from 2 to 18°.[16] To elucidate the mechanism of water droplet removal, further investigation into dynamic hydrophobicity is necessary.

The removability of water droplets deteriorates due to pinning. Droplet pinning occurs on surfaces that are geometrically uneven or chemically heterogeneous. There are several reports on dynamic hydrophobicity on geometrically uneven surfaces.[12,17] Kurogi *et al.* pointed out that pinning occurs at the transition from protrusions to recesses on surfaces with fine irregularities.[17] Periodic microstructured surfaces with uniform chemical properties have been demonstrated using a self-assembled monolayer.[18] It was noted that during the evaporation of droplets on these microstructured surfaces, pinning occurs due to the micropillars.[18] Yoshimitsu *et al.* investigated the dynamic hydrophobicity of a silicon wafer surface machined with periodic grooves and coated with a fluorine-based coating.[12] The sliding angle increases when droplets fall orthogonal to the grooves, as opposed to parallel, because of the occurrence of pinning. Long *et al* used femtosecond lasers to create a rice-leaf-like groove microstructure on the surface.[19] Consistent with Yoshimitsu *et al.*'s findings, the sliding angle is larger when droplets fall orthogonal to the grooves than in the parallel direction owing to the occurrence of pinning.[12]

There are several reports on the dynamic hydrophobicity of chemically heterogeneous surfaces. Li *et al.* pointed out that chemical heterogeneity occurs at boundaries where surface properties change.[20] Song *et al.* reported that pinning occurs at the coating interface due to heterogeneity when applying two fluorine-based coatings in a line pattern.[11]

Murase and Fujibayashi pointed out that compared with fluorine-based coatings, silicone-based coatings display unique wettability characteristics.[21] Despite silicone-based coatings having lower contact angles, water droplets slide more easily on their surfaces than on fluorine-based ones.[21] This suggests that the reduced mobility of water molecules on the surfaces of fluorine-based coatings could be attributed to the rigidity induced in the assembly of water molecules on a fluoro segment.[21] In recent years, concerns have arisen regarding the accumulation of organic fluorinated compounds, present in fluorine-based coatings, in both the human body and the environment.[22] Consequently, silicone-based coatings have attracted attention as an alternative lubricating material.

In this study, our objective is to fabricate a silicone-based surface featuring chemically homogeneous and geometrically uniform properties for droplet sliding. This surface was designed to reduce both the k value in Eq. (1) and the CAH, leading to lower F_r. Until now, no surface with a uniaxial microgroove structure that does not cause pinning has been fabricated. The molding process was used to fabricate uniaxial groove structures on the silicone surface, allowing control over the periodicity. The sliding angle and F_c were investigated, and the effect of structural parameters on the dynamic hydrophobicity was systematically studied. Furthermore, the F_r acting on the droplet was theoretically analyzed to explain the observed phenomena. Note that this study is limited to the sliding behavior of water droplets on the surface.

2. Materials and Methods

Molds with various structures were prepared by dicing flat silicon wafers with a dicing machine (DAD-3240, DISCO Inc., Japan). The dicing blade (ZHZZ, DISCO Inc., Japan) was rotated at 25000 rpm and the dicing rate was 40 mm/s. Silicone (KE-111, Shin-etsu Silicone Co., Japan) was used as the hydrophobic sheets. To further enhance the silicone sheet hydrophobicity, microlines were printed by the molding process. All the molds were first cleaned to remove any particles that may have escaped sonication. The molding processes were carried out at 60 °C for 8 h. The mold and the work area with fine grooves on the silicone sheet both cover an area of 25 × 25 mm^2. To investigate the impact of the raised line pitch on the contact angle of the fabricated surface, the width of the raised line on the silicone sheet (hereafter referred to as the raised line width) was maintained at a constant value of 9 ± 0.6 μm. Meanwhile, the pitch of the side walls between adjacent line structures (hereafter referred to as the raised line pitch) was varied, with values set at 30, 60, and 90 μm. Figure 2 shows the laser micrographs of the microgroove structure on the silicone sheets prepared by the molding process. The sheets with the microgrooves are referred to as Pitch30, Pitch60, and Pitch90 sheets, corresponding to the pitches of 30, 60, and 90 μm, respectively. A sheet using an unprocessed silicon wafer as a mold is called a flat sheet. Contact ratios represent the proportion of the raised line width to the raised line pitch. Thus, the contact ratios between the droplet and the silicone surfaces were 0.3, 0.15, and 0.1. The following equation shows the contact ratio when the contact ratio between the flat sheet surface and a water droplet is set to 1:

$$C_r = w/p, \tag{2}$$

where C_r, w, and p denote the contact ratio, raised line width, and raised line pitch, respectively.

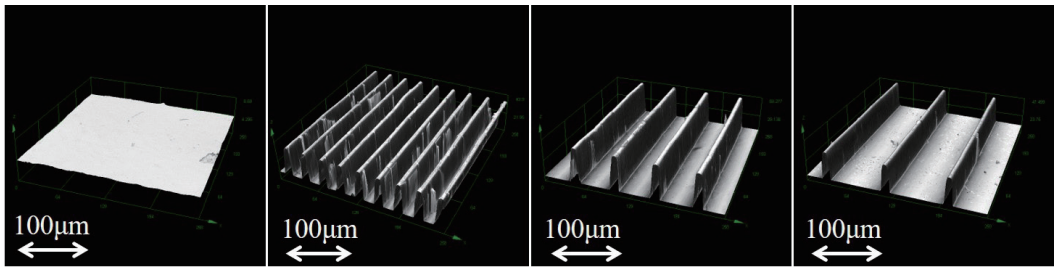

$Ra = 0.64 \pm 0.06$			
Flat sheet	Pitch30 sheet	Pitch60 sheet	Pitch90 sheet
Raised line pitch p[μm]	30.0 ± 0.5	60.0 ± 0.3	90.0 ± 0.4
Raised line width w[μm]	9.1 ± 0.5	9.1 ± 0.4	9.0 ± 0.4
Raised line height h[μm]	33.0 ± 0.3	37.9 ± 0.2	32.7 ± 0.2
(a)	(b)	(c)	(d)

Fig. 2. Laser microscopy images of the microgroove structure on the silicone sheet: (a) flat sheet, (b) Pitch30 sheet, (c) Pitch60 sheet, and (d) Pitch90 sheet.

The microstructure was observed and evaluated on a laser scanning microscope (OLS4100, Olympus Co., Japan). The sessile drop method was used for contact angle measurements on a commercial contact angle meter (FTA 1000, First Ten Angstroms, Inc., USA). The volume of water droplets used for the measurements was 10 μL. For each sample, six points were examined in two directions: orthogonal and parallel to the longitudinal axis of the microgroove, as illustrated in Fig. 3. Sliding angles of water droplets were measured using a commercial sliding angle measurement system (Fta32, First Ten Angstroms, Inc., USA). The volume of water droplets for these measurements was 10 μL. The sliding angles were measured from five different points for each sample, and average values were calculated.

3. Results and Discussion

Figure 4 shows photographs of a 10 μL water droplet on the prepared microgroove structures, taken from a direction orthogonal to the microgroove, with corresponding water contact angles and the contact-line width. Figure 4 indicates that the water contact angle increases with increasing raised line pitch. The water droplet contacted the entire surface of the flat sheet.

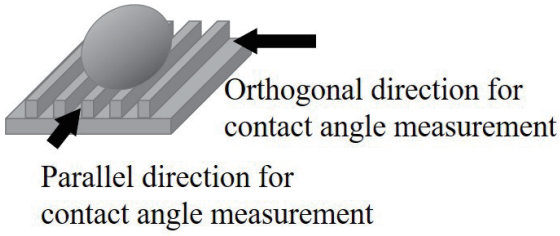

Fig. 3. Schematic illustration of the measurement directions on the groove structure to determine the contact angle.

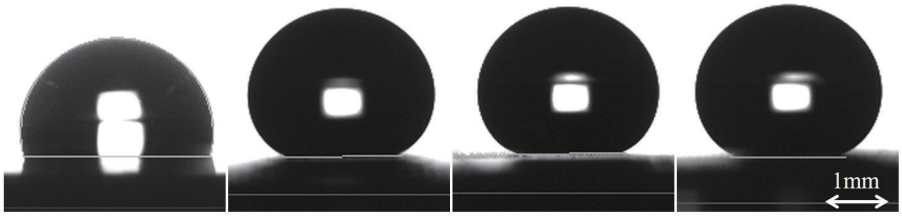

		Flat sheet	*Pitch30 sheet*	*Pitch60 sheet*	*Pitch90 sheet*
Contact angle θ [deg]	Othogonal	104.7 ± 2.0	130.8 ± 4.7	138.3 ± 0.1	137.5 ± 0.8
	Parallel	-	132.3 ± 0.4	131.9 ± 2.4	133.2 ± 1.1
Contact-line width 2r [mm]		3.00 ± 0.16	2.02 ± 0.08	1.74 ± 0.11	1.78 ± 0.02
		(a)	(b)	(c)	(d)

Fig. 4. Orthogonal view of water droplet shapes on the microgroove structures, with the corresponding water contact angles θ and contact-line widths 2r noted below each image: (a) flat sheet, (b) Pitch30 sheet, (c) Pitch60 sheet, and (d) Pitch90 sheet.

Conversely, the water contact angle on the microgroove structure becomes higher and remains constant, and the contact-line width also becomes shorter. Trapped air was observed at the interface between the water droplet and the silicone sheet with the microgroove structure, indicating the dominance of Cassie's mode, which refers to a composite wetting state where the air is trapped within the surface microstructures.[23]

Figure 5 shows the relationship between the distance traveled by the rear end point of a water droplet and the tilt angle when the silicone sheet surface is inclined so that the droplet slides along the raised line. Water droplets on the flat sheet surface appear to slide out at an inclination angle of approximately 10°. Figure 6 shows the average sliding angles for each type of silicone sheet. Error bars represent the maximum and minimum sliding angles observed. The silicone sheets with the microgroove structure had the sliding angle of less than 5°, while the Pitch90 sheet had a sliding angle of 1.9°. Yoshimitsu *et al.* reported that the sliding angle of water droplets parallel to the grooves on the silicon wafer surface was more than 42°. In their study, the raised line width, raised line pitch, and raised line height were 96, 145, and 160 μm,

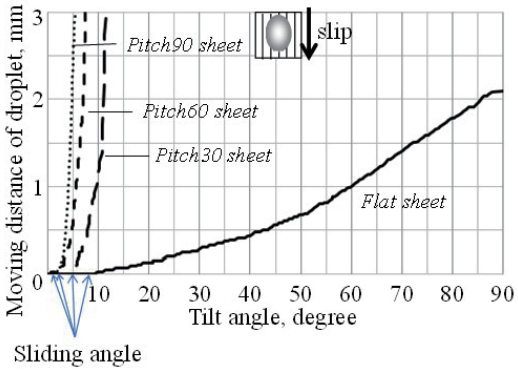

Fig. 5. (Color online) Relationship between the distance moved by the rear end point of a water droplet and the tilt angle when the silicone sheet surface is inclined, causing the droplet to slide along the raised line. Line types represent different sheet types: solid line for flat sheet, long dashed line for Pitch30 sheet, dashed line for Pitch60 sheet, and dotted line for Pitch90 sheet.

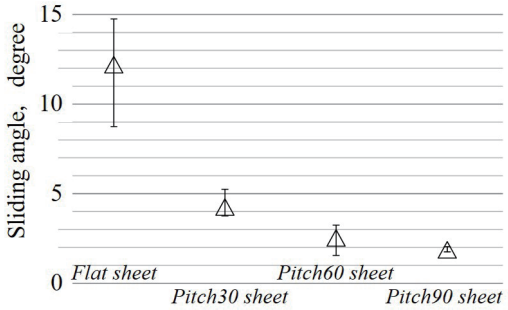

Fig. 6. Average sliding angles for each type of silicone sheet, with error bars indicating the maximum and minimum sliding angles observed: flat sheet, Pitch30 sheet, Pitch60 sheet, and Pitch90 sheet.

respectively.[12] The smaller sliding angle that was observed in our study compared with that reported by Yoshimitsu *et al.* can be attributed to two factors: (1) the raised line width of the microgroove sheet in our study is approximately 1/10 of that in Yoshimitsu *et al.*'s study,[12] and (2) the silicone base material used in our study does not reduce the mobility of water molecules.[21]

Figure 7 shows a photograph of the water droplets on the flat sheet surface and on the Pitch60 sheet surface, with the left side of the image indicating the direction of sliding. The experimental apparatus used for observing the droplets employs a synchronized mechanism where both the stage and the camera tilt simultaneously. This setup gives the appearance that the droplets are situated on a horizontal plane in the captured images. The left side of the image corresponds to the downslope of the inclination, causing the droplets to tilt leftward. The advancing contact angle, represented by the left side of the droplet, was approximately equal to the static contact angle, while the receding contact angle, represented by the right side of the droplet, was smaller than the static contact angle. This observation was consistent with the notion that silicone does not reduce the mobility of water molecules.[21] Figure 8 shows the average CAH of water droplets

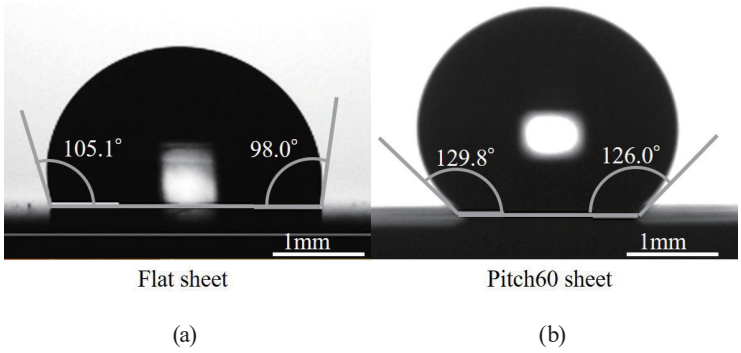

Fig. 7. Photograph of water droplets on the flat sheet surface and the Pitch60 sheet surface, with the left side of the image indicating the direction of sliding and the corresponding advancing (right side) and receding (left side) contact angles: (a) flat sheet and (b) Pitch60 sheet.

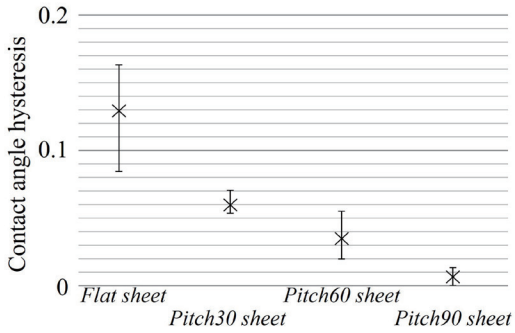

Fig. 8. Average contact angle hysteresis (CAH) of the water droplets on each sheet type, with error bars representing the maximum and minimum values: flat sheet, Pitch30 sheet, Pitch60 sheet, and Pitch90 sheet. The decrease in CAH with increasing raised line pitch is attributed to the increased amount of trapped air in the grooves and reduced contact ratio between the water droplets and the top of the raised lines.

on each sheet, with error bars representing the maximum and minimum values. Compared with the flat sheet surface, the silicone sheet with the microgroove structure displayed reduced CAH. The CAH decreases with increasing raised line pitch. This decrease in CAH is attributed to the increase in the amount of trapped air in the grooves, which indicates that the contact ratio between the water droplets and the top of the raised line is reduced.

Figure 9 shows the relationship between F_c or F_r, and the contact ratio. F_c and F_r are given by the following equations.

$$F_c = mg\sin\alpha \tag{3}$$

$$F_r = \frac{48}{\pi} r\gamma\left(\cos\theta_r - \cos\theta_a\right) \tag{4}$$

F_c and F_r were consistent. Elsherbini and Jacobi found that F_c on plane surfaces with contact angle differences, defined as the difference between advancing and receding angles, ranging from 23° to 51°, were proportional to the product of the contact-line width and the CAH.[8] Our study demonstrates that for the silicone sheet with the microgroove structure, where the contact angle differences are small, F_c on the surface exhibits a similar trend to the results reported by Elsherbini and Jacobi.[8] In the sliding behavior of liquid droplets on a hydrophobic surface, the two main sliding modes are well known: the rolling and slipping modes. Suzuki *et al.* pointed out the ratio of the slipping mode decreases with increasing number of pinning points.[24] Despite the different CAH, the similarity in the results can be attributed to the slipping mode. However, to confirm the reliability of this explanation, a more detailed investigation is required.

F_c and F_r are found to be proportional to the contact ratio. F_r of the silicone sheet with microgroove structures and the water droplet can be expressed by the following equation when F_r of a flat sheet and the water droplet is F_f.

$$F_r = C_r F_f \tag{5}$$

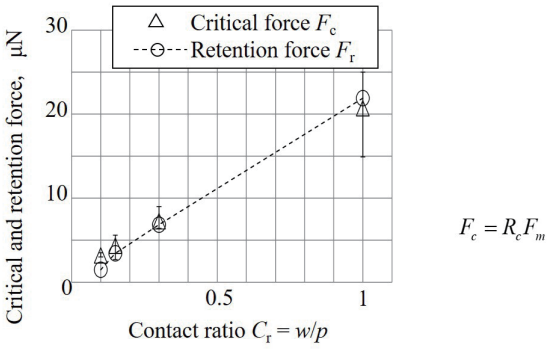

Fig. 9. Relationship between F_c or F_r and the contact ratio for the silicone sheets: flat sheet, Pitch30 sheet, Pitch60 sheet, and Pitch90 sheet. F_c and F_r exhibit a consistent trend across different sheet types.

Water droplets on the silicone sheet with microgroove structures are considered to be in the Cassie mode. It is thought that the decrease in F_r is due to a reduction in the contact area or line, which results from a decrease in the contact ratio. If F_r of the flat sheet and the water droplet is determined, F_r of the silicone sheet with the microgroove structure and the water droplet can be controlled by adjusting the contact ratio.

4. Conclusions

In this study, to design a surface that minimizes F_r, a silicone-based surface with chemically homogeneous and geometrically uniform properties suitable for droplet sliding was fabricated. A uniaxial groove structure was fabricated on the silicone surface using a molding process, allowing control over the periodicity. The sliding angles and F_c were investigated, and the effects of the contact-line width and the CAH were systematically studied. Additionally, the F_r acting on the droplets was theoretically analyzed.

In conclusion, the results of this study have successfully demonstrated the following points.

1. The silicone sheet with the microgroove structure exhibits a smaller CAH than a flat sheet surface, which affects the behavior of water droplets on the surface.
2. F_c and F_r on the silicone sheet with the microgroove structure are proportional to the contact ratio, allowing for the adjustment of F_r by controlling the contact ratio.
3. The results show that trapped air in the groove decreases the contact ratio between the droplet and the surface. This decrease in the contact ratio leads to a reduction in both the contact-line width and the CAH, which in turn decreases F_r. Consequently, the decrease in Fr results in a reduced sliding angle.

Our findings are consistent with those of Elsherbini and Jacobi, who demonstrated that F_c on plane surfaces with large contact angle differences were proportional to the product of the contact-line width and the CAH.[8] Out results extend their results by showing a similar trend for F_c on the silicone sheet with the microgroove structure, where the contact angle differences are small. The size of the work area with the microgrooves on the silicone sheet is currently constrained by the working space of the dicer. In the future, the use of technology such as laser processing machines is expected to expand this working area.

This research has provided valuable insights into the sliding behavior of water droplets on silicone sheets with microgroove structures, and it has potential applications in various fields such as self-cleaning surfaces, anti-icing systems, and semiconductor processes.

Acknowledgments

This work was supported by JSPS KAKENHI Grant Number 18K03905.

References

1 A. Nakajima: NPG Asia Mater. **3** (2011) 49. https://doi.org/10.1038/asiamat.2011.55
2 N. Janardan and M. V. Panchagnula: Colloids Surf., A **456** (2014) 238. https://doi.org/10.1016/j.colsurfa.2014.05.051

3 J. J. Bikerman: J. Colloid Sci. **5** (1950) 349. https://doi.org/10.1016/0095-8522(50)90059-6
4 C. G. L. Furmidge: J. Colloid Sci. **17** (1962) 309. https://doi.org/10.1016/0095-8522(62)90011-9
5 A. Carre and M. E. R. Shanahan: J. Adhesion. **49** (1995) 177. https://doi.org/10.1080/00218469508014354
6 R. A. Brown, F. M. Orr Jr., and L. E. Scriven: J. Colloid Interface Sci. **73** (1980) 76. https://doi.org/10.1016/0021-9797(80)90124-1
7 C. W. Extrand and Y. Kumagai: J. Colloid Interface Sci. **170** (1995) 515. https://doi.org/10.1006/jcis.1995.1130
8 A. I. ElSherbini and A. M. Jacobi: J. Colloid Interface Sci. **273** (2004) 556. https://doi.org/10.1016/j.jcis.2003.12.067
9 C. W. Extrand: Langmuir **32** (2016) 8608. https://doi.org/10.1021/acs.langmuir.6b02292
10 R. David and A. W. Neumann: Colloids Surf., A **393** (2012) 32. https://doi.org/10.1016/j.colsurfa.2011.10.020
11 J.-H. Song, M. Sakai, N. Yoshida, S. Suzuki, Y. Kameshima, and A. Nakajima: Surf. Sci. **600** (2006) 2711. https://doi.org/10.1016/j.susc.2006.04.044
12 Z. Yoshimitsu, A. Nakajima, T. Watanabe, and K. Hashimoto: Langmuir **18** (2002) 5818. https://doi.org/10.1021/la020088p
13 W. Barthlott and C. Neinhuis: Planta **202** (1997) 1. https://doi.org/10.1007/s004250050096
14 L. Feng, S. Li, Y. Li, H. Li, L. Zhang, J. Zhai, Y. Song, B. Liu, L. Jiang, and D. Zhu: Adv. Mater. **14** (2002) 1857 https://doi.org/10.1002/adma.200290020
15 L. Feng, Y. Zhang, J. Xi, Y. Zhu, N. Wang, F. Xia, and L. Jiang: Langmuir **24** (2008) 4114. https://doi.org/10.1021/la703821h
16 Y. Wang and B. Bhushan: ACS Appl. Mater. Interfaces **7** (2015) 743. https://doi.org/10.1021/am5067755
17 K. Kurogi, H. Yan, and K. Tsujii: Colloid. Surf., A **317** (2008) 592. https://doi.org/10.1016/j.colsurfa.2007.11.048
18 D. I. Yu, H. J. Kwak, S. W. Doh, H. C. Kang, H. S. Ahn, K. Moriyama, H. S. Park, and M. H. Kim: Int. J. Heat Mass Transfer **90** (2015) 191. https://doi.org/10.1016/j.ijheatmasstransfer.2015.06.046
19 J. Long, P. Fan, D. Jiang, J. Han, Y. Lin, M. Cai, H. Zhang, and M. Zhong: Adv. Mater. Interfaces **3** (2016) 1600641. https://doi.org/10.1002/admi.201600641
20 Q. Li, P. Zhou, and H. J. Yan: Langmuir **32** (2016) 9389. https://doi.org/10.1021/acs.langmuir.6b01490
21 H. Murase and T. Fujibayashi: Prog. Org. Coat. **31** (1997) 97. https://doi.org/10.1016/S0300-9440(97)00023-4
22 Z. Zheng, H. Yu, W.-C. Geng, X.-Y. Hu, Y.-Y. Wang, Z. Li, Y. Wang, and D.-S. Guo: Nature Commun. **10** (2019) 5762. https://doi.org/10.1038/s41467-019-13775-1
23 A. B. D. Cassie and S. Baxter: Trans. Faraday Soc. **40** (1944) 546. https://doi.org/10.1039/TF9444000546
24 S. Suzuki, A. Nakajima, M. Sakai, Y. Sakurada, N. Yoshida, A. Hashimoto, Y. Kameshima, and K. Okada: Chem. Lett. **37** (2008) 58. https://doi.org/10.1246/cl.2008.58